Received 23 July 2023; accepted 13 September 2023. Date of publication 20 September 2023; date of current version 4 October 2023.

Digital Object Identifier 10.1109/OJAP.2023.3317409

Design of Compact and High Isolation Dual-Polarized Antenna Array via Plasmonic Meta-Structure

ZHANG WEN CHENG[1], SHIMENG WANG[2], YUE TENG CHEN[1], JI RAN CHEN[1], JING CHENG LIANG[1], FENG GAO[2], SHUAI LUAN[2], XIN LIU[2], HUI FENG MA[1] (Member, IEEE), AND TIE JUN CUI[1] (Fellow, IEEE)

[1]State Key Laboratory of Millimeter Waves, School of Information Science and Engineering, Southeast University, Nanjing 210096, China

[2]China Mobile R&D Center for Network Planning and Optimization, China Mobile Group Design Institute Company Ltd., Beijing 100080, China

CORRESPONDING AUTHOR: H. F. MA (e-mail: hfma@seu.edu.cn)

This work was supported in part by the National Science Foundation of China under Grant 62071117, Grant 61831006, and Grant 62288101; in part by the Postgraduate Research and Practice Innovation Program of Jiangsu Province under Grant KYCX23-0253; in part by the Major Project of the Natural Science Foundation of Jiangsu Province under Grant BK20212002; in part by 111 Project under Grant 111-2-05; in part by the Project for Jiangsu Specially-Appointed Professor; in part by the China Mobile Group Design Institute Company Ltd.–Southeast University Joint Laboratory under Grant CMDI-202100604; and in part by the Fundamental Research Funds for the Central Universities under Grant 2242023K5002.

(Zhang Wen Cheng and Shimeng Wang contributed equally to this work.)

ABSTRACT We propose a compact and high isolation dual-polarized antenna array based on plasmonic meta-structure operating at 2.58 GHz. The compact principle of the dual-polarized antenna is mainly based on spoof surface plasmon polariton (SSPP) radiation patch to support SSPP modes, which is fed by spatially coupled excitation. Due to the slow-wave feature of SSPPs, the size of dual-polarized radiation patch is reduced to $0.2\lambda_0 \times 0.2\lambda_0$, and the total antenna size is reduced to $0.39\lambda_0 \times 0.39\lambda_0$, which is much smaller than that of the traditional microstrip antenna with $0.5\lambda_0 \times 0.5\lambda_0$. The cross-polarization coupling between two polarization ports can be improved to below -32 dB, showing high isolation characteristics. Besides, a 3×3 compact antenna array is also designed, fabricated, and measured to verify the feasibility of its extension to larger-scale antenna systems. Both simulated and measured results of the proposed compact antenna and the antenna array illustrate compact profiles, good $\pm45^\circ$ radiation performance, and high isolation levels, which have potential application values for the massive multiple-input and multiple-output (MIMO) base stations.

INDEX TERMS Compact antenna, high isolation, dual polarizations, spoof surface plasmon polaritons (SSPPs), multiple-input and multiple-output (MIMO).

I. INTRODUCTION

Massive multiple input and multiple output (MIMO) has increasingly become an indispensable technique in base stations of the future communication systems. It can significantly improve spectral efficiency, diversity performance, and independent data streams existing between the transmitters and receivers by adopting multiple antennas [1]. As the main element of the MIMO antenna array, dual-polarized antenna can provide polarization diversity, improve channel capacity, and alleviate multipath fading [2], [3], [4]. However, multiple dual-polarized antennas are always bulky and heavy to form an array, which bring a series of challenges in miniaturized massive MIMO system.

Over the past decade, various methods have emerged to design miniaturized and compact dual-polarized antennas [5], [6], [7], [8], [9], [10], [11], [12], [13], [14], [15], [16], which can integrate more antennas in a limited space, and thereby improving the channel capacity and spectrum efficiency of the existing communication systems to support more users [17]. In [5], [6], [7], aperture coupling stacked patches are applied to change the conditions of the boundary surface, which reshape the radiation performance and miniaturize the antennas. However, these improvements are made at the expense of height, bandwidth, and gain. In [8], [9], [10], dual polarization dielectric resonator antennas have been proposed with the advantages of low loss, compact size, and light weight. The high-dielectric constant materials increase process cost and make the array too bulky for large-scale integration. In addition, high back-lobe radiation and low gain are the main imperfections faced by most dielectric resonator antennas. In [11] and [12], magnetoelectric dipole antennas make frontward radiation fields coincide and the backward radiations weaken, but their miniaturization abilities are very limited. Folding dipole antennas can also transfer resonance frequency to a lower operating band by installing parasitic elements to provide compact antenna structure with enhanced bandwidth [13], [14]. In addition, metamaterials have been introduced to realize antenna miniaturization and radiation performance improvement simultaneously [15], [16]. In [16], a compact flat antenna has been proposed, which can operate at lower frequencies without increasing its physical size by introducing metamaterial units below the radiation patch. However, those metamaterial-based antennas only reduce the radiation patches effectively, rather than their overall profiles, which are unsuitable for large-scale manufacturing.

Spoof surface plasmon polaritons (SSPPs) are special surface electromagnetic (EM) waves with strong confinements existing in the low frequency bands (e.g., terahertz, millimeter wave, and microwave) [18], [19], [20], [21], which can mimic similar characteristics of surface plasmon polaritons (SPPs) in the optical frequency [22], [23]. Due to the properties of ultra-thin structure [24] and great compatibility with planar circuit [25], the SSPP-based structures have been widely applied in antenna designs, such as leaky-wave antennas [26], [27], [28], endfire antennas [29], [30], patch antennas [31], [32], and helical antenna [33]. It has been proved that the slow-wave characteristic of SSPPs can be used for miniaturization design [31], [32], [33], [34], [35], [36]. However, to the best of authors' knowledge, the designs of dual-polarized antenna and its array application based on SSPPs have not been reported yet.

In this paper, a compact dual-polarized antenna array based on SSPPs is proposed. The antenna consists of dual-polarized SSPP-based radiation patch excited by a spatially coupled feeding structure and vertical metallic walls (MWs). Due to the slow-wave characteristic of SSPPs, the radiation patch size and total antenna size are effectively reduced to $0.2\lambda_0 \times 0.2\lambda_0$ and $0.39\lambda_0 \times 0.39\lambda_0$, respectively. Simulated results of the compact dual-polarized SSPP antenna are verified by measurements, showing good ±45° radiation characteristics and high isolation level within the operating frequency band. Then, a 3×3 compact antenna array is fabricated and measured to verify the feasibility of its extension to larger-scale antenna systems. The proposed SSPP antenna has significant advantages of compact size and high capacity, which has potential applications in the MIMO base stations.

II. COMPACT PRINCIPLE AND ANTENNA DESIGN

The configuration of the ±45° radiation patch based on SSPPs is illustrated in Figure 1(a), which is a cross-shaped

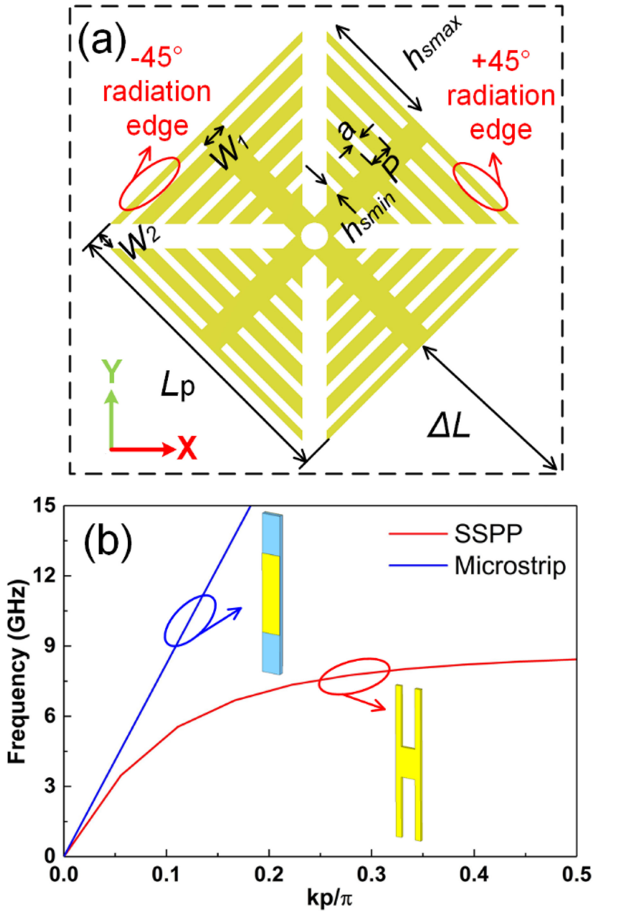

FIGURE 1. **(a) Configuration of the SSPP radiation patch where P=1.8 mm, a=1 mm, W_1=2 mm, W_2=1.3 mm, and L_p=24 mm. (b) Dispersion curves of the traditional microstrip structure and the SSPP structure.**

corrugated metallic path composed of several SSPP units whose h_s varies evenly from the edge (h_{smax}=9.7 mm) to center (h_{smin}=0.9 mm). The simulated dispersion curves of traditional microstrip structure and SSPP structure are depicted in Figure 1(b), in which the SSPP line uses the average value of SSPP units with different h_s. It can be observed that the dispersion curve of SSPP structure deviates increasingly away from that of traditional microstrip line at a fixed frequency, which means that the larger propagation constant can be achieved at a fix frequency, showing significant slow-wave characteristic. According to the patch antenna theory [37], the operating frequency and relevant dimension parameters of the typical TM_{10} mode can be obtained by

$$f_r = \frac{1}{2L_p\sqrt{\varepsilon_p\mu_p} + 4\Delta L\sqrt{\varepsilon_0\mu_0}\sqrt{\varepsilon_{ref}\mu_{ref}}} \tag{1}$$

$$\varepsilon_{ref} = \frac{\varepsilon_r + 1}{2} + \frac{\varepsilon_r - 1}{2}\left[1 + 12h/L_p\right]^{-1/2},\ \ \mu_{ref} = \mu_r = 1 \tag{2}$$

$$\frac{\Delta L}{h} = 0.412\frac{\left(\varepsilon_{ref} + 0.3\right)\left(\frac{L_p}{h} + 0.264\right)}{\left(\varepsilon_{ref} - 0.258\right)\left(\frac{L_p}{h} + 0.8\right)} \tag{3}$$

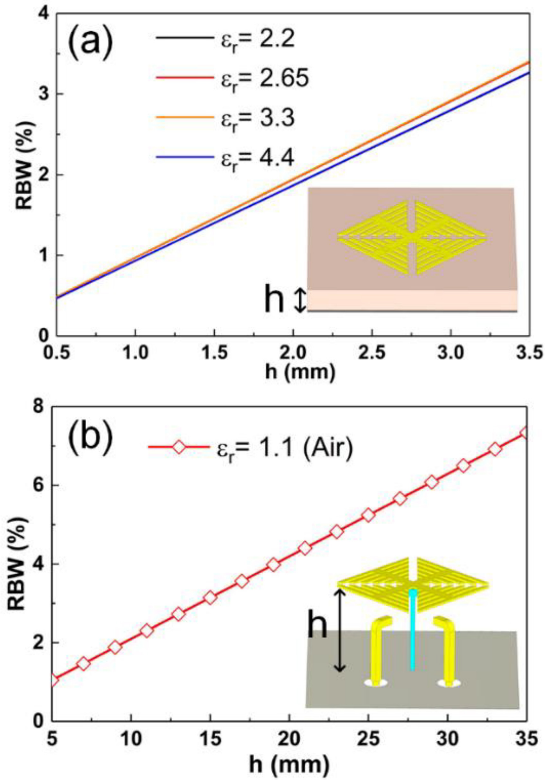

FIGURE 2. Calculated RBWs of (a) the normal patch antenna using dielectric materials with different permittivities (ε_r) and (b) the spatially coupled excited antenna according to the change of *h* at 2.58 GHz.

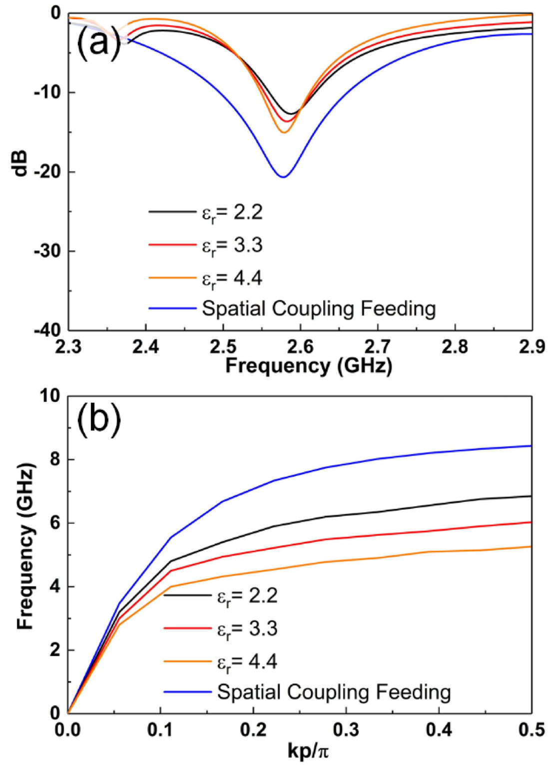

FIGURE 3. Simulated (a) reflection coefficients and (b) dispersion curves of the SSPP unit using different dielectric substrates (thickness of 2 mm) and spatial coupling feeding (patch height of 25 mm).

where ε_{p} and μ_{p} are the average permittivity and permeability of the metal SSPP patch, $\varepsilon_{\mathrm{ref}}$ and μ_{ref} are the equivalent relative permittivity and permeability of the fringing capacitance structure (without metal patch), and ε_{r} and μ_{r} are the relative permittivity and permeability of the material below the patch. Besides, h, L_{p}, and ΔL are the patch height, patch length, and the fringing capacitance length, respectively.

Compared to microstrip structure, SSPP structure has a larger propagation constant (k_x), which is calculated by:

$$k_x = w\sqrt{\varepsilon_p \mu_p} \tag{4}$$

where w represents the angular frequency. The larger k_x means the larger $\varepsilon_{\mathrm{p}}\mu_{\mathrm{p}}$, then the smaller f_{r} can be achieved according to (1), so that the antenna can have smaller electrical dimension, resulting in a more compact size.

Bandwidth performance is one of important indicators for dual-polarized antenna, and the relative bandwidth (RBW) of the proposed SSPP antenna can be calculated by [37]

$$RBW = 3.77\left((\varepsilon_r - 1)/\varepsilon_r^2\right)(W/L)(h/\lambda_0) \cdot\sqrt{\left(\varepsilon_{ref}\mu_{ref}\varepsilon_0\mu_0\right)/\left(\varepsilon_p\mu_p\right)} \tag{5}$$

Figure 2(a) shows the calculated RBWs of the dual-polarized microstrip antenna using dielectric substrates with different permittivities (ε_{r}) according to the change of h at 2.58 GHz. It can be found that with the introduction of a larger k_x by SSPPs, the RBWs always maintain within a low range of below 2% for different common dielectric materials with thickness $h \leq 2$ mm. Although the RBWs can be improved by increasing h, it will cause difficulties in manufacturing and higher processing cost, as well as makes the antenna too bulky to be applied. Figure 2(b) illustrates the calculated RBWs of the antenna using spatially coupled manner according to the change of h (patch height) at 2.58 GHz. Two L-shaped probes and a nylon dielectric column are used to feed and fix the SSPP patch, respectively, resulting in the permittivity of the equivalent dielectric material below the patch becoming slightly larger than ε_0, which is approximately set as 1.1. The energy from input ports is fed into the L-probes, and then coupled to the metallic SSPP patch. It can be seen that by spatial coupling feeding, the RBW can be increased to more than 5% regardless of height limitation. The schematic configurations of the normal microstrip antenna and the spatially coupled excited antenna are also shown in the inset of Figures 2(a) and (b), respectively. Figure 3(a) shows the simulated reflection coefficients of antenna using different dielectric substrates (with permittivities of 2.2, 3.3, and 4.4) and spatial coupling feeding, which indicates the same bandwidth expansion effect by spatial coupling feeding as Figure 2. Besides, Figure 3(b) illustrates simulated dispersion curves of SSPP for the two types of design schemes. It

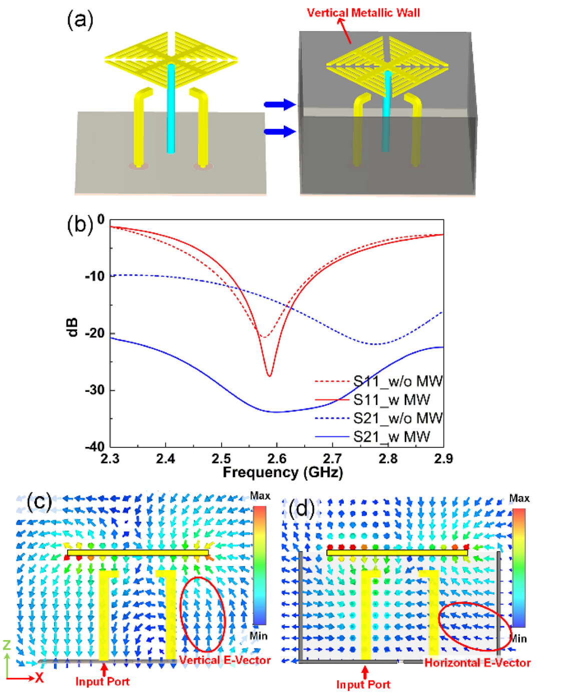

FIGURE 4. (a) Configuration of the dual-polarized antenna without and with MWs. (b) Simulated reflection coefficients and isolation coefficients without and with MWs. (c) Simulated vector electric field distributions without MWs in the *xoz* plane. (d) Simulated vector electric field distributions with MWs in the *xoz* plane.

can be seen that the effect on miniaturization by using high-permittivity dielectrics always occurs in the higher frequency range, which can be replaced by spatial coupling feeding on the desired 2.58 GHz without affecting the premise of miniaturization.

Another important performance for dual-polarized antenna is the isolation level between the two polarizations, which can be improved effectively by using MWs to surround the antenna. Figure 4(a) shows the configuration of the dual-polarized antenna without and with surrounding MWs, whose height is equal to patch height and the thickness is 1 mm. Figure 4(b) illustrates the simulated reflection coefficients and isolation coefficients of the antennas without and with MWs. It can be seen that the MWs hardly cause deviation of the resonance frequency from the reflection coefficients (S_{11}), while the isolation coefficients (S_{21}) are observably reduced from -11 dB to -35 dB. Moreover, to further reveal the underlying working mechanisms of the decoupling method, the simulated vector electric field distributions of the antenna in the *xoz* plane without and with MWs are shown in Figures 4(c) and (d), respectively. As is shown in Figure 4(c), without MWs, the vector electric field is directed from the ground plane towards the patch, which is almost parallel to the probe placed vertically, resulting in large coupling effect. On the contrary, by using MWs with the same height as patch, the position of zero electric potential (ground plane) is raised, making the vertical component of the vector electric field greatly reduced shown in Figure 4(d), which leads to lower coupling.

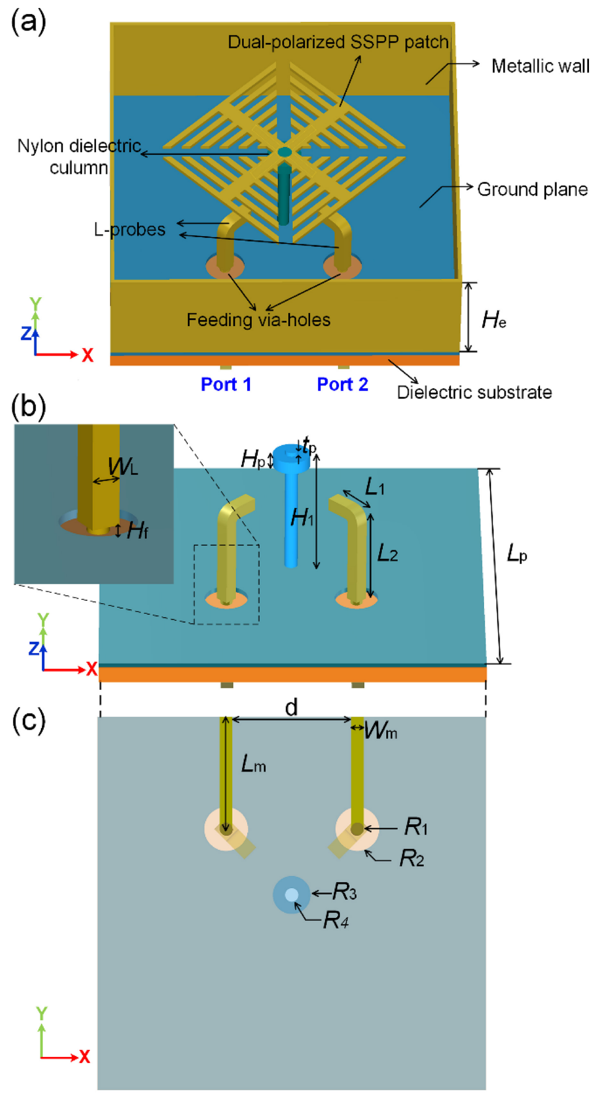

FIGURE 5. (a) Schematic configuration of the proposed dual-polarized SSPP antenna. (b) Structure of the feeding part where L_1=4.5 mm, L_2=26 mm, W_L=2 mm, H_f=0.5 mm, H_1=30 mm, and H_p=3 mm. (c) Bottom view where R_1=0.75 mm, R_2=2.59 mm, R_3=2.3 mm, R_4=1 mm, W_m= 2R_1=1.5 mm, L_m=15.2 mm, and d=16 mm.

III. DESIGN, FABRICATED, AND MEASUREMENT OF COMPACT SSPP ANTENNA

The schematic configuration of the proposed compact dual-polarized antenna is shown in Figure 5(a), which is composed of a SSPP radiation patch, metallic walls, and a spatially coupled feeding part as discussed above. As shown in Figure 5(b), the feeding part consists of a nylon dielectric column, two L-shaped copper probes with a bend angle of 90°, and a two-port microstrip structure whose dielectric substrate is Rogers RT5880 with relative permittivity of 2.2, loss tangent of 0.0009, and thickness of 0.508mm, as shown in Figure 5(c). The port impedance of feeding via-hole is designed as 50 Ω, which is connected to the bottom 50-Ω input feeding microstrip line. The SSPP radiation patch with thickness of t_p=1 mm is installed by the

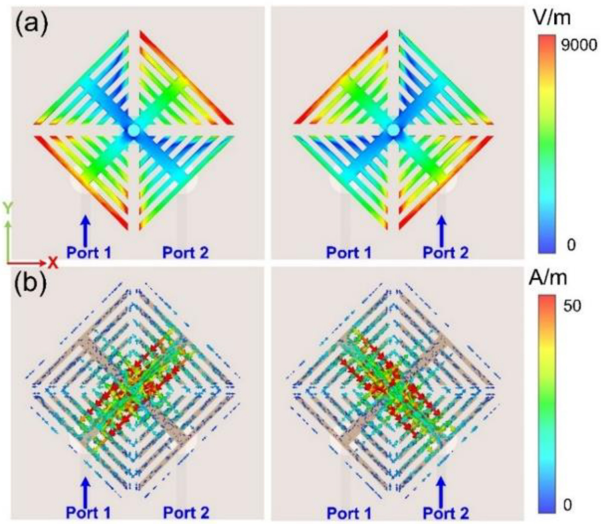

FIGURE 6. Simulated (a) electric field distributions and (b) surface currents on the top layer of the SSPP antenna at 2.58 GHz.

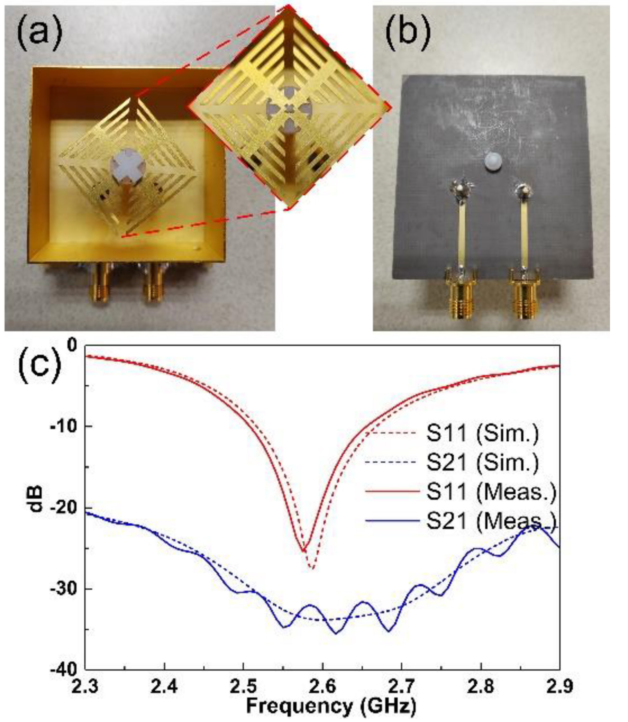

FIGURE 7. Photographs of the fabricated compact antenna. (a) Top layer. (b) Bottom layer. (c) Simulated and measured *S*-parameters.

nylon dielectric column directly above the metal ground and fed through L-shaped probes. When f_r=2.58 GHz is chosen as the operation frequency, k_x= 69.4 m^{-1} can be obtained from dispersion curve and $(\varepsilon_p\mu_p)^{1/2}$= 4.3×10^{-9} s/m can be calculated from (5). The L-probe coupling feeding design can be regarded as a microstrip transmission structure with air-dielectric substrate, then $\varepsilon_{ref}=\mu_{ref}=1$ can be calculated from (2). In addition, the side length of SSPP patch is $L_p=2h_{smax}+W_1+2W_2$=24 mm, which is only about 0.2λ_0 at 2.58 GHz. Substituting all the above parameters into (1), the edge length ΔL=13.7 mm can be calculated, and $H_1=H_e\approx$28 mm can be obtained from (3) as well. After all the parameters are determined, we can calculate the antenna length L_t=45 mm, whose total size is 0.39$\lambda_0\times$0.39λ_0. Figure 6 demonstrates the full-wave simulated electric field distributions and the surface currents on the top layer of the proposed SSPP antenna for +45° (Port 1) and −45° (Port 2) feeding, respectively. As shown in Figure 6(a), the electric fields are larger at the radiation-edge (±45°-edge) compared to those at the middle, which is attributed to radiating current flowing mainly along the radiation-direction (±45°-direction), as shown in Figure 6(b). Besides, electric fields around both radiation edges of each polarization have identical amplitudes but opposite phases. Hence, it can be concluded that the radiation mode is the normal dipole mode, whose operating frequency is determined by the propagation constant and the physical length of the radiation patch along the ±45°-direction for each polarization.

To validate the analysis above, the proposed compact SSPP antenna is fabricated and measured. Figures 7(a) and (b) show the top view and bottom view of the fabricated antenna, respectively, in which a small cross groove is etched in the middle of the patch by a nylon button, allowing the patch to be better fixed on the nylon medium column by using a nylon buckle. Both simulated and measured *S*-parameters are provided in Figure 7(c). The reflection coefficients (S_{11}) are lower than −10 dB from around 2.52 to 2.64 GHz, showing the −10dB RBW is 5.4%, which is consistent with the theoretical value in Figure 3(b). The isolation coefficients (S_{21}) are around −32 dB or lower, illustrating high isolation characteristics within the operating frequency band. Figures 8(a)-(c) illustrate the simulated and measured 2D far-field radiation patterns of E-plane and H-plane at 2.58 GHz when port 1 is fed at frequencies of 2.53 GHz, 2.58 GHz, and 2.63 GHz, respectively. It can be seen that all the measured gains in the *z*-direction are above 5.3 dBi, showing a good agreement with the simulated results. Besides, the cross-polarization lower than −25 dB is observed over the operation band, which demonstrates good radiation performance. The measured gains are slightly lower than those of simulations due to the errors in complex sample fabrication, assembly processes, as well as the welding errors of the vertical copper MWs. Figure 9 demonstrates the simulated and measured gains and the simulated total efficiencies of the compact antenna, showing the gains near the center operating frequency are larger than 5.5 dBi, and the radiation efficiencies are almost larger than 85% in whole frequency band from 2.52 to 2.64 GHz. All the results indicate the high-efficiency radiations around the operating frequency.

Table 1 summarizes the performance comparison between the proposed dual-polarized antenna and some related works. Compared with antennas printed on dielectric substrates [7], [8], [11], the SSPP antenna has obvious advantages in patch size and total size, which avoids the use

TABLE 1. Comparison between the proposed SSPP antenna and some published dual-polarized works.

Ref.	Operating Frequency (GHz)	RBW (%)	Patch Size ($\lambda_0\times\lambda_0$)	Total Size ($\lambda_0\times\lambda_0$)	Dielectric Thickness (mm)/ε_r	Patch Height (λ_0)	Center Gain (dBi)	Isolation Level (dB)
[7]	3.62-3.77	4	0.29×0.29	1×1.06	3.7/2.2	/	NG	32
[8]	2.50-2.76	9.9	0.34×0.34	0.5×0.5	7/38	/	5.6	43
[11]	1.62-2.87	56	0.48×0.48	1.0×1.0	4/5.7	/	8.8	30
[13]	0.69-0.96	16.4	0.28×0.28	NG	/	0.29	9	25
[14]	1.58-2.77 4.71-6.18	54.71/27	0.3×0.3/ 1.0×1.0	0.68×0.68/ 1.7×1.7	/	0.29/0.72	10/10	41/35
[16]	1.67-1.88 1.91-2.24	11.8/15.9	0.29×0.6/ 0.32×0.68	0.98×1.37 1.12×1.56	/	0.1/0.08	12.5/13	28/28
This work	**2.52-2.64**	**5.4**	**0.2×0.2**	**0.39×0.39**	**/**	**0.24**	**5.7**	**32**

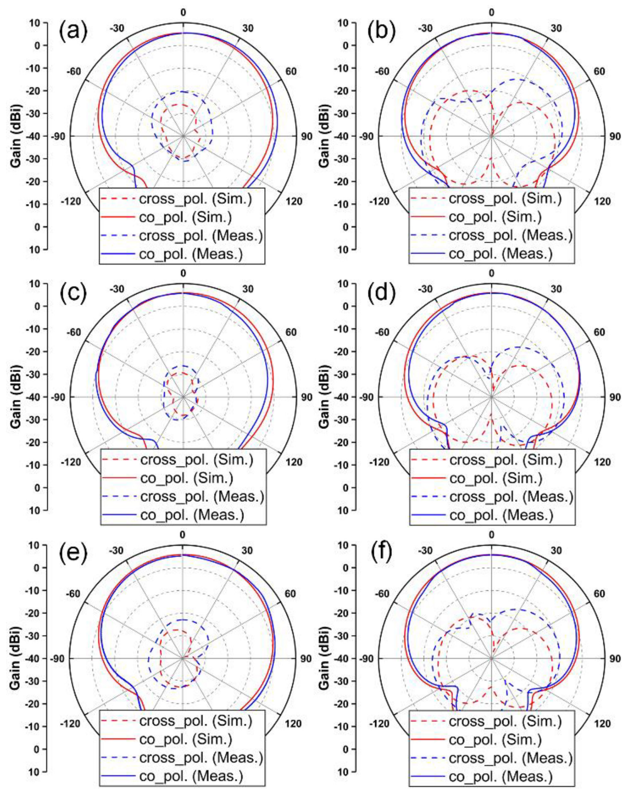

FIGURE 8. Simulated and measured radiation patters of SSPP antenna. (a) E-plane and (b) H-plane at 2.53 GHz. (c) E-plane and (d) H-plane at 2.58 GHz. (e) E-plane and (f) H-plane at 2.63 GHz.

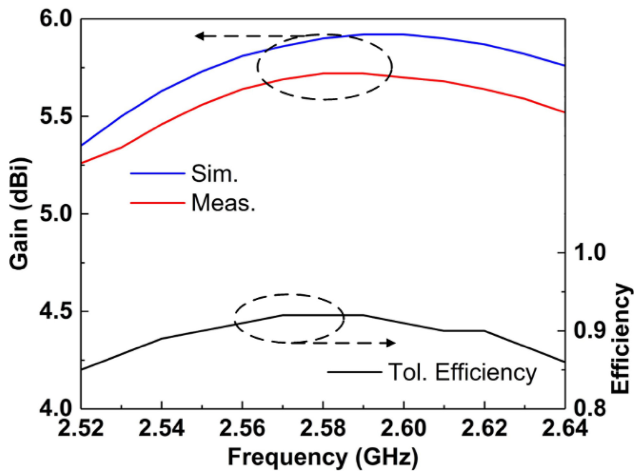

FIGURE 9. Simulated and measured gains and simulated total efficiencies.

of expensive and bulky dielectric materials. One the other hand, compared with the compact designs without dielectric substrates in [13], [14], and [16], the compression of the overall profile is more obvious. Thus, by applying SSPP technology, the dual-polarized antenna has been verified to be designed in an ultra-compact size effectively.

IV. DESIGN, MEASUREMENT, AND DISCUSSION OF ANTENNA ARRAY

As described in Introduction part, the advantages of miniaturized antenna will be even more obvious in the array applications. Specifically, due to the size reduction of antenna elements in an array, more antennas can be placed in a fix area, which will increase the number of communication channels and increase the communication capacity for the larger-scale array. However, for most existing miniaturized antennas [5], [6], [7], [8], [9], [10], [11], [12], [13], [14], [15], [16], [31], [32], [33], their performance and application in arrays have not been discussed and verified yet. Therefore, in this section, the array designed based on compact antennas and potential problems (e.g., complex feeder layout and mutual coupling effect) in practical applications will be discussed in detail.

As an example, a 3×3 six-port SSPP antenna array is fabricated, whose top and bottom views are shown in Figures 10(a) and (b), respectively. Since the distance between adjacent antennas is compressed to $0.39\lambda_0$, the feeding lines need to be arranged flexibly in a small area to ensure that the feeder branches do not overlap and have high isolation. As is shown in Figure 10(b), the bottom feeding network consisting six independent series-fed microstrip lines is designed, which meets the requirement

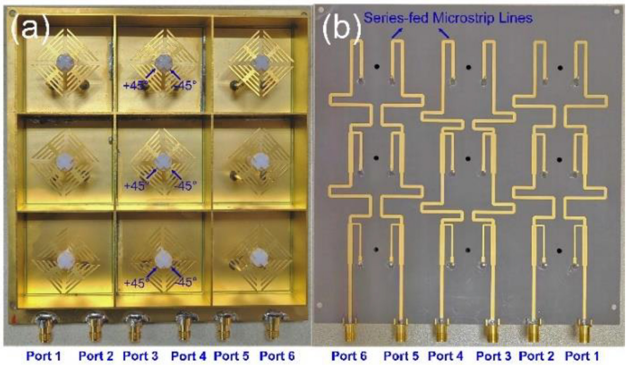

FIGURE 10. **Photographs of the fabricated 3×3 six-ports SSPP antenna array. (a) Top View. (b) Bottom View.**

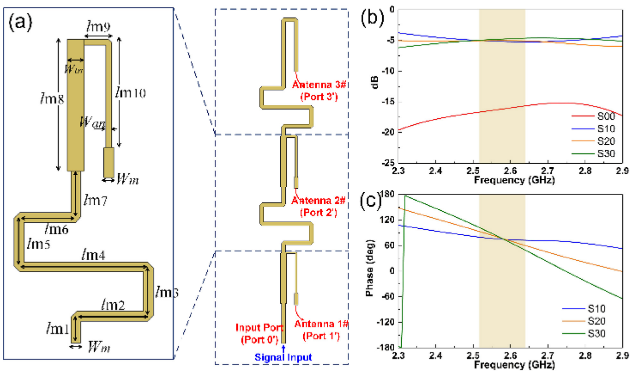

FIGURE 11. **(a) Geometry of series-fed microstrip line where W_m=1.5 mm, W_{a1}=0.75 mm, W_{t1}=2.23 mm, W_{a2}=1.3 mm, W_{t2}=2.49 mm, W_{a3}=1.5 mm, W_{t3}=1.5 mm, l_{m1}=5 mm, l_{m2}=8 mm, l_{m3}=8 mm, l_{m4}=19 mm, l_{m5}=6 mm, l_{m6}=11 mm, l_{m7}= 6.4mm, l_{m8}= 21.1mm, l_{m9}=5.3 mm and l_{m10}=15.3 mm, l'_{m1}=2.5 mm, l'_{m2}=8 mm, l'_{m3}=3 mm, l'_{m4}=19 mm, l'_{m5}=4 mm, l'_{m6}=11 mm, and l'_{m7}=15.9 mm. (b) Simulated amplitudes of *S*-parameters where S_{00} is the reflection coefficient Port 0' and S_{i0} (i=1, 2, 3) are the transmission coefficients of Port 1', Port 2', and Port 3', respectively. (c) Simulated transmission phases of S_{i0}.**

of independent transceiver components according to the distinctive feature of massive integrated MIMO array in practical applications. Among these series-fed lines, Port 1, Port 3, and Port 5 are connected to +45°-polarization radiation, while Port 2, Port 4, and Port 6 are used to feed −45°-polarization radiation, respectively, whose initial widths remain W_m, satisfying 50-Ω impedance matching. Assuming that the energy received by Antenna n# is P_n (n=1, 2, 3), and R is the ratio of the energy propagated to the subsequent antennas to Antenna n#, the design guidelines for series-fed microstrip lines are as follow:

$$\left(\sum_{i=1+n}^{3} P_i\right)/P_n = R \tag{6}$$

$$Z_{tn} = \sqrt{\sqrt{R}/\left(\sqrt{R}+1\right)Z_0} \tag{7}$$

$$Z_{an} = \sqrt[4]{R}\cdot Z_0 \tag{8}$$

in which Z_{tn} and Z_{an} correspond to the impedances of branches width W_{tn} and W_{an}, respectively, which are used

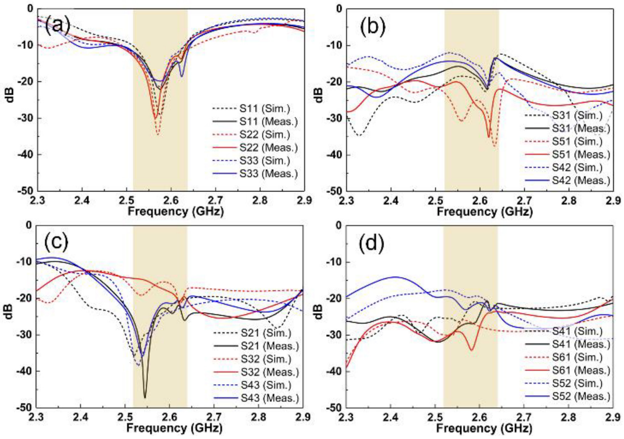

FIGURE 12. **Simulated and measured *S*-parameters of the antenna array. (a) Reflection coefficients. (b) Co-polarization coupling. (c) Cross-polarization coupling between adjacent ports. (d) Cross-polarization coupling between nonadjacent ports.**

to control the output amplitudes. In our design, Z_0 is 50-Ω characteristic impedance and P_1:P_2:P_3 is set as 1:1:1, then the widths W_{tn} and W_{an} can be calculated according to (6)–(8) and comprehensive formulas of the microstrip line. The lengths l_{mj} (j=1, 2, 3, . . . , 8) are used to control the output phases, in which $\sum_{j=1}^{7} l_{mj} = 3/4\lambda_g$ and l_{m8}= $1/4\lambda_g$ (λ_g is guided wavelength of microstrip line), respectively. Besides, the $l_{m9}+l_{m10}$ should remain unchanged for all antennas without any length limitation. Obviously, for l_{mj} (j=1, 2, 3, . . . , 7), we have enough flexibility to define length of each branch, which provides the basis for designing feeders in compact array. Therefore, two kinds of feeding lines are designed as shown in Figure 11(a), in which $\sum_{j=1}^{7} l_{mj}$ is used for Port 1, Port 2, Port 5, and Port 6, and $\sum_{j=1}^{7} l'_{mj}$ is used for Port 3 and Port 4, whose simulated output amplitudes and phases are illustrated in Figures 11(b) and (c), respectively, showing good energy distribution effect and in-phase feed around center operating frequency. It should be noted that this design method can be extended to the feeding line with more output terminals, and the output amplitudes and phases can be arbitrarily designed as required.

The fabricated 3×3 antenna array is fully measured. During the measurements, the ports without feeding signals are terminated by 50-Ω matching loads. Only *S*-parameters fed from port 1, port 2, and port 3 are presented due to the symmetry of antenna array. The simulated and measured *S*-parameters of the array are shown in Figure 12. According to the results in Figure 12(a), all the reflection coefficients remain at −10 dB or better within the whole operating frequency band from 2.52 to 2.64 GHz, which illustrates a good match with the results of the single antenna. Figure 12(b) illustrates that the isolation coefficients between adjacent ports (S_{31} and S_{42}) are lower than −13 dB while the co-polarization isolation coefficients between nonadjacent ports (S_{51}) are less than −20 dB. The cross-polarization isolation coefficients are shown in Figures 12(c) and (d),

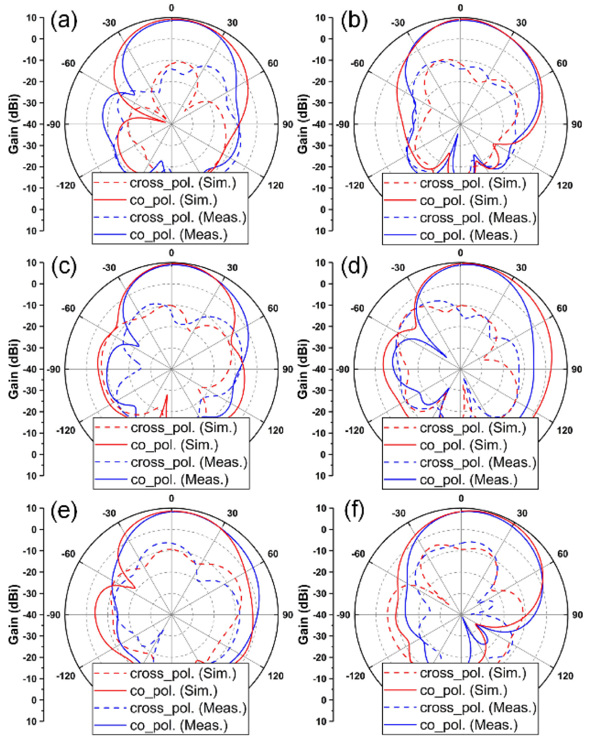

FIGURE 13. Simulated and measured radiation patters of the antenna array at 2.58 GHz. (a) E-plane and (b) H-plane when port 1 is excited. (c) E-plane and (d) H-plane when port 2 is excited. (e) E-plane and (f) H-plane when port 3 is excited.

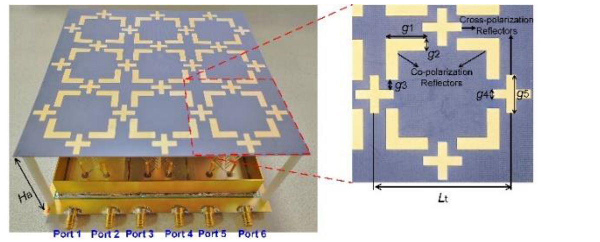

FIGURE 14. Schematic configuration of the fabricated antenna array with DS where L_t=45 mm, H_a=40 mm, g_1=14 mm, g_2=4 mm, g_3=3.5 mm, g_4=3 mm, and g_5=13 mm.

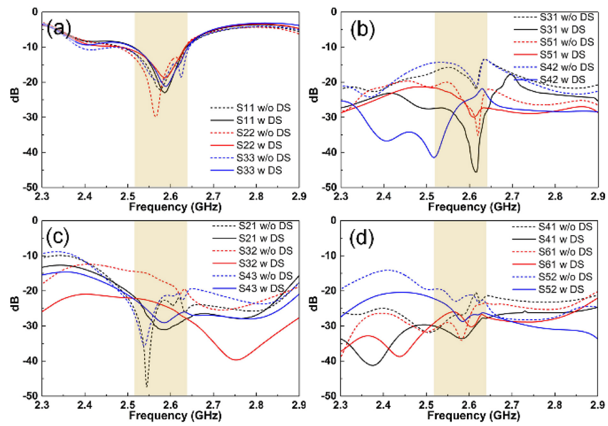

FIGURE 15. Measured *S*-parameters of the antenna array without and with DS. (a) Reflection coefficients. (b) Co-polarization coupling. (c) Cross-polarization coupling between adjacent ports. (d) Cross-polarization coupling between nonadjacent ports.

indicating that the cross-polarization isolation coefficients can be maintained at a low level of below −20 dB for antenna itself (S_{21}, S_{43}) and nonadjacent antennas (S_{41}, S_{61}, and S_{52}), which will remain below –15dB for adjacent antennas (S_{32}). It can be concluded that all the isolation coefficients are maintained at a low level, especially for antenna itself and non-adjacent input ports. Figure 13 shows the radiation patterns of *E*-planes and *H*-planes at 2.58 GHz, illustrating the gains of all ports are above 8 dBi. The measured results are in good agreement with the simulated results, indicating good radiation performance with −17 dB cross-polarization.

Through the measured results, it can be seen that the whole antenna array has compact overall profile and good radiation performance, but there is only a defect that the adjacent antennas have a slightly larger coupling level (around −13 dB). In fact, the designed 3×3 array can cover all the coupling cases in a large-scale array, which contains a central antenna element surrounded by eight elements, four side antenna elements and four corner antenna elements. Therefore, the coupling characteristics of a larger-scale antenna array can be directly evaluated from the designed 3×3 array.

V. FURTHER PERFORMANCE IMPROVEMENT BY ADOPTING DECOUPLING SURFACE

In this section, we designed a decoupling surface (DS) to further improve decoupling effect of the MIMO antenna array, thereby achieving better system performance [41], [42], [43], [44], [45], [46], [47], [48], [49]. The schematic configuration of the antenna array covered with a DS is shown in Figure 14. The DS unit consists of several equilateral L-shaped and cross-shaped metal reflectors, which are printed on a 1 mm-thick dielectric substrate of F4BM265 with the relative permittivity of 2.65 and loss tangent of 0.001. The L-shaped and cross-shaped metallic structures are designed to suppress co-polarization and cross-polarization coupling, respectively.

Then the antenna array with the DS is measured in the same test environment. The comparisons of the measured S-parameters of the array without and with DS are shown in Figure 15. It can be seen that −10 dB bandwidth within the operating frequency band is achieved for all ports as shown in Figure 15(a), illustrating that the DS almost has no influence on the desired resonance of the array. Figure 15(b) illustrates the co-polarization coupling isolations between adjacent antennas (S_{31} and S_{42}) can be improved by around 15 dB to over 22 dB, while the co-polarization isolation between nonadjacent antennas (S_{51}) remains at a high level of over 22 dB by loading DS. Figure 15(c) illustrates all the cross-polarization isolation coefficients between two adjacent ports can be improved to below −23 dB, in which the improvement of adjacent ports (S_{32}) is particularly significant. In fact, the cross-polarization coupling of the antenna itself maintains high levels (S_{21} and S_{43}), while the DS

TABLE 2. Comparison between the proposed antenna array and other published arrays using DS techniques.

Ref.	Frequency (GHz)	Element Distance (λ_0)	DS Height (λ_0)	Isolation (dB)	Antenna Type	Complexity of DS	Array Configuration
[46]	4.23-4.82	0.5	0.45	24	Patch Antenna	Single	4×4
[47]	3.3-3.8	0.71	0.33	25	Monopole	Single	2×2
[49]	3.3-3.8	0.5	0.4	25	Staggered Dipole	Complicated	4-4-4-4
This work	**2.52-2.64**	**0.39**	**0.24**	**22**	**Patch Antenna**	**Simple**	**3×3**

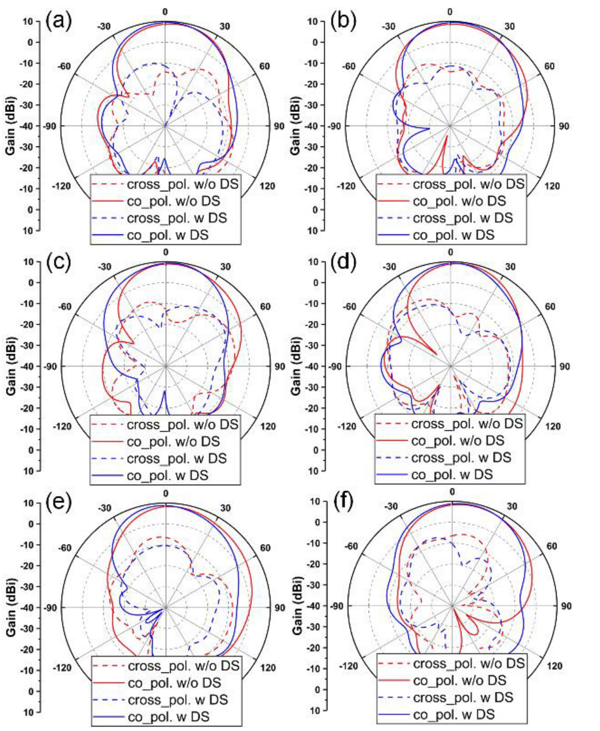

FIGURE 16. Measured radiation patters of the antenna array without and with DS at 2.58 GHz. (a) E-plane and (b) H-plane when port 1 is excited. (c) E-plane and (d) H-plane when port 2 is excited. (e) E-plane and (f) H-plane when port 3 is excited.

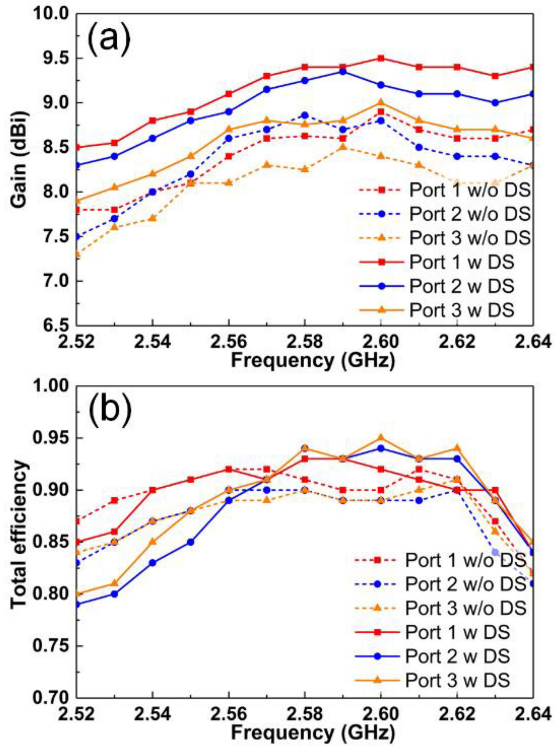

FIGURE 17. (a) Measured gains and (b) simulated total efficiencies of the antenna array without and with DS.

is mainly used for decoupling the adjacent antennas (S_{32}). Figure 15(d) demonstrates that the cross-polarization isolation coefficients between two nonadjacent ports are all improved to below -23 dB, and the closer the distance between antennas, the more significant the improvement effect. Figure 16 shows the measured radiation patterns at 2.58 GHz, showing that the beam widths basically maintain the same with or without DS, but the radiation directions are almost corrected to $+z$ direction due to the reduction of mutual coupling. Besides, the results illustrate that good cross-polarization ratios can be retained, which are better than -19 dB for all input ports. Figures 17(a) and (b) demonstrate the measured gains and simulated efficiencies. Since the mutual coupling are reduced effectively by DS and more power is radiated along the normal direction ($+z$ direction), the gains and total efficiencies are slightly enhanced as well, in which the gains are enhanced by around 0.6 dB and the total efficiencies are almost larger than 80% within the operating frequency band from 2.52 to 2.64 GHz.

We have also compared the proposed antenna array with previously reported works using DS techniques, as shown in Table 2. It can be found that the proposed array not only exhibits of compact size, but also has a lower overall profile than other arrays which benefits from the strong binding of SSPP modes. Therefore, the proposed compact antenna array not only has significant advantages in the miniaturized element size and compact overall size when a DS is loaded, but also can still keep a high isolation level.

VI. CONCLUSION

In this paper, a compact dual-polarized SSPP antenna array has been designed, fabricated, and measured. The implementation of the miniaturized antenna mainly relies on the large propagation constant of SSPPs, which reduces the patch size and the total size to $0.2\lambda_0 \times 0.2\lambda_0$ and $0.39\lambda_0 \times 0.39\lambda_0$, respectively. By using spatially coupled excitation and vertical MWs, the RBW and isolation level and of the antenna reach around 5.7% and above 32 dB, effectively. Besides, a 3×3 compact antenna array has been fabricated and measured, showing good radiation performance and compact overall profile. Both simulated and measured results indicate that the SSPP-based compact antenna has significant advantages of compact patch size and total profile, which can be extended to design larger-scale antenna array. It is expected that the proposed design has strong practical application values in highly integrated massive MIMO base stations.

REFERENCES

[1] E. Björnson, J. Hoydis, and L. Sanguinetti, "Massive MIMO has unlimited capacity," *IEEE Trans. Wireless Commun.*, vol. 17, no. 1, pp. 574–590, Jan. 2018.

[2] S. C. Wen, Y. Z. Xu, and Y. D. Dong, "A low-profile dual-polarized omnidirectional antenna for LTE base station applications," *IEEE Trans. Antennas Propag.*, vol. 19, no. 7, pp. 1078–1082, Sep. 2021.

[3] R. Wu and Q. X. Chu, "A compact, dual-polarized multiband array for 2G/3G/4G base stations," *IEEE Trans. Antennas Propag.*, vol. 67, no. 4, pp. 2298–2304, Apr. 2019.

[4] H. Q. Zhai, L. Xi, Y. Q. Zang, and L. Li, "A low-profile dual-polarized high-isolation MIMO antenna arrays for wideband base-station applications," *IEEE Trans. Antennas Propag.*, vol. 66, no. 1, pp. 191–202, Jan. 2018.

[5] S. K. Padhi, N. C. Karmakar, C. L. Law, and S. Aditya, "A dual polarized aperture coupled circular patch antenna using a C-shaped coupling slot," *IEEE Trans. Antennas Propag.*, vol. 51, no. 12, pp. 3295–3298, Dec. 2003.

[6] S. Gao, L. W. Li, M. S. Leong, and T. S. Yeo, "A broad-band dual-polarized microstrip patch antenna with aperture coupling," *IEEE Trans. Antennas Propag.*, vol. 51, no. 4, pp. 898–900, Apr. 2003.

[7] Y. Gao, R. Ma, Y. Wang, Q. Zhang, and C. Parini, "Stacked patch antenna with dual-polarization and low mutual coupling for massive MIMO," *IEEE Trans. Antennas Propag.*, vol. 64, no. 10, pp. 4544–4549, Oct. 2016.

[8] H. Tang, C. W. Tong, and J. X. Chen, "Differential dual-polarized filtering dielectric resonator antenna," *IEEE Trans. Antennas Propag.*, vol. 66, no. 8, pp. 4298–4302, Aug. 2018.

[9] X. Y. Wang, S. C. Tang, L. L. Yang, and J. X. Chen, "Differential-fed dual-polarized dielectric patch antenna with gain enhancement based on higher order modes," *IEEE Antennas Wireless Propag. Lett.*, vol. 19, no. 3, pp. 502–506, Mar. 2020.

[10] M. D. Rotaru and J. K. Sykulski, "Design and analysis of a novel compact high permittivity dielectric resonator antenna," *IEEE Trans. Magn.*, vol. 45, no. 3, pp. 1052–1055, Mar. 2009.

[11] S. Zhou, Z. Peng, G. Huang, and C. Sim, "Design of a novel wide-band and dual-polarized magnetoelectric dipole antenna," *IEEE Trans. Antennas Propag.*, vol. 65, no. 5, pp. 2645–2649, May 2017.

[12] Y. Zhang, X. Y. Zhang, and Q. H. Liu, "Dual-Polarized filtering magnetoelectric dipole antenna utilizing intrinsic highpass filter network and integrated lowpass filter network," *IEEE Trans. Antennas Propag.*, vol. 69, no. 12, pp. 8090–8099, Dec. 2021.

[13] J.-H. Ou, Z. Chen, S. F. Bo, Y. Zhang, and X. Y. Zhang, "Compact dual-polarized antenna with low-pass response for marine communication," *IEEE Trans. Veh. Technol.*, vol. 70, no. 3, pp. 2649–2656, Mar. 2021.

[14] W. Wang, S. Yang, Z. Fang, Q. Sun, Y. Chen, and Y. Zheng, "Compact dual-polarized wideband antenna with dual-/single-band shifting for microbase station applications," *IEEE Trans. Antennas Propag.*, vol. 69, no. 11, pp. 7323–7332, Nov. 2021.

[15] S. A. Rezaeieh, M. A. Antoniades, and A. M. Abbosh, "Miniaturization of planar Yagi antennas using Mu-negative metamaterial-loaded reflector," *IEEE Trans. Antennas Propag.*, vol. 65, no. 12, pp. 6827–6837, Dec. 2017.

[16] M. Li, Q. Li, B. Wang, C. Zhou, and S. Cheung, "A miniaturized dual-band base station array antenna using band notch dipole antenna elements and AMC reflectors," *IEEE Trans. Antennas Propag.*, vol. 66, no. 6, pp. 3189–3194, Jun. 2018.

[17] M. A. Jensen and J. W. Wallace, "A review of antennas and propagation for MIMO wireless communications," *IEEE Trans. Antennas Propag.*, vol. 52, no. 11, pp. 2810–2824, Nov. 2004.

[18] J. B. Pendry, "Mimicking surface plasmons with structured surfaces," *Science*, vol. 305, no. 5685, pp. 847–848, Aug. 2004.

[19] F. J. Garcia-Vidal, L. Martín-Moreno, and J. B. Pendry, "Surfaces with holes in them: New plasmonic metamaterials," *J. Opt. A Pure Appl. Opt.*, vol. 7, no. 2, pp. S97–S101, Feb. 2005.

[20] A. P. Hibbins, B. R. Evans, and J. R. Sambles, "Experimental verification of designer surface plasmons," *Science*, vol. 308, no. 5722, pp. 670–672, Apr. 2005.

[21] F. J. Garcia-Vidal et al., "Spoof surface plasmon photonics," *Rev. Mod. Phys.*, vol. 94, no. 2, 2022, Art. no. 25004.

[22] H. Reather, "Surface plasmons on smooth and rough surfaces and on gratings," *Springer Tracts in Modern Physics*, vol. 111. Berlin, Germany: Springer-Verlag, 1988, pp. 1–3.

[23] W. L. Barnes, A. Dereux, and T. W. Ebbesen, "Surface plasmon subwavelength optics," *Nature*, vol. 424, no. 6950, pp. 824–830, Aug. 2003.

[24] X. Shen, T. J. Cui, D. Martin-Cano, and F. J. Garcia-Vidal, "Conformal surface plasmons propagating on ultrathin and flexible films," *Proc. Nat. Acad. Sci.*, vol. 110, no. 1, pp. 40–45, Jan. 2013.

[25] H. F. Ma, X. Shen, Q. Cheng, W. X. Jiang, and T. J. Cui, "Broadband and high-efficiency conversion from guided waves to spoof surface plasmon polaritons," *Laser Photon. Rev.*, vol. 8, no. 1, pp. 146–151, Jan. 2014.

[26] M. Wang, H. F. Ma, H. C. Zhang, W. X. Tang, X. R. Zhang, and T. J. Cui, "Frequency-fixed beam-scanning leaky-wave antenna using electronically controllable corrugated microstrip line," *IEEE Trans. Antennas Propag.*, vol. 66, no. 9, pp. 4449–4457, Sep. 2018.

[27] M. Wang, H. F. Ma, W. X. Tang, H. C. Zhang, W. X. Jiang, and T. J. Cui, "A dual-band electronic-scanning leaky-wave antenna based on a corrugated microstrip line," *IEEE Trans. Antennas Propag.*, vol. 67, no. 5, pp. 3433–3438, May 2019.

[28] Z. W. Cheng, H. F. Ma, M. Wang, and T. J. Cui, "Dual-beam leaky-wave radiations with independent controls of amplitude, angle, and polarization based on SSPP waveguide," *Adv. Photon. Res.*, vol. 3, Jan. 2022, Art. no. 2100313.

[29] S. Li, Q. Zhang, Z. Xu, H. Zhao, and X. Yin, "Phase transforming based on asymmetric spoof surface plasmon polariton for endfire antenna with sum and difference beams," *IEEE Trans. Antennas Propag.*, vol. 68, no. 9, pp. 6602–6613, Sep. 2020.

[30] Y. Han et al., "Shared-aperture antennas based on even- and odd-mode spoof surface plasmon polaritons," *IEEE Trans. Antennas Propag.*, vol. 68, no. 4, pp. 3254–3258, Apr. 2020.

[31] J. Lu, H. C. Zhang, P. H. He, L. P. Zhang, and T. J. Cui, "Design of miniaturized antenna using corrugated microstrip," *IEEE Trans. Antennas Propag.*, vol. 68, no. 3, pp. 1918–1924, Mar. 2020.

[32] J. Lu, H. C. Zhang, C. Wei, J.-S. Hong, and T. J. Cui, "Design of compact circularly polarized antenna using sunshine-shaped slotted patch," *IEEE Trans. Antennas Propag.*, vol. 68, no. 9, pp. 6800–6805, Sep. 2020.

[33] Z. W. Cheng et al., "A compact axial-mode helical antenna based on spoof surface plasmon polaritons," *IEEE Trans. Antennas Propag.*, vol. 71, no. 7, pp. 5582–5590, Jul. 2023.

[34] M. Wang, S. Sun, H. F. Ma, and T. J. Cui, "Supercompact and ultra-wideband surface plasmonic bandpass filter," *IEEE Trans. Microw. Theory Techn.*, vol. 68, no. 2, pp. 732–740, Feb. 2020

[35] B. C. Pan, G. Q. Luo, Z. Liao, J. L. Cai, and B. G. Cai, "Wideband miniaturized design of complementary spoof surface plasmon polaritons waveguide based on interdigital structures," *Sci. Rep.*, vol. 10, no. 1, pp. 1–7, Feb. 2020.

[36] L. Ye, Y. Chen, Z. Wang, C. Zhu, J. Zhuo, and Q. H. Liu, "Compact spoof surface plasmon polariton waveguides and notch filters based on meander-strip units," *IEEE Photon. Technol. Lett.*, vol. 33, no. 3, pp. 135–138, Feb. 2021.

[37] C. A. Balanis, *Antenna Theory Analysis and Design*, 3rd ed. Hoboken, NJ, USA: Wiley, 2005, pp. 812–826.

[38] H. Wong, K.-L. Lau, and K.-M. Luk, "Design of dual-polarized L-probe patch antenna arrays with high isolation," *IEEE Trans. Antennas Propag.*, vol. 52, no. 1, pp. 45–52, Jan. 2004.
[39] C. L. Mak, K. M. Luk, K. F. Lee, and Y. L. Chow, "Experimental study of a microstrip patch antenna with an L-shaped probe," *IEEE Trans. Antennas Propag.*, vol. 48, no. 5, pp. 777–783, May 2000.
[40] Y. X. Guo, C. L. Mak, K. M. Luk, and K. F. Lee, "Analysis and design of L-probe proximity fed-patch antennas," *IEEE Trans. Antennas Propag.*, vol. 49, no. 2, pp. 145–149, Feb. 2001.
[41] L. Savy and M. Lesturgie, "Coupling effects in MIMO phased array," in *Proc. IEEE Radar Conf. (RadarConf)*, Philadelphia, PA, USA, May 2016, pp. 1–6.
[42] Q. Yuan, Q. Chen, and K. Sawaya, "Performance of adaptive array antenna with arbitrary geometry in the presence of mutual coupling," *IEEE Trans. Antennas Propag.*, vol. 54, no. 7, pp. 1991–1996, Jul. 2006.
[43] B. Wang, Y. Chang, and Y. Sun, "Performance of the large-scale adaptive array antennas in the presence of mutual coupling," *IEEE Trans. Antennas Propag.*, vol. 64, no. 6, pp. 2236–2245, Jun. 2016.
[44] C. Masouros, M. Sellathurai, and T. Ratnarajah, "Large-scale MIMO transmitters in fixed physical spaces: The effect of transmit correlation and mutual coupling," *IEEE Trans. Commun.*, vol. 61, no. 7, pp. 2794–2804, Jul. 2013.
[45] K.-H. Chen and J.-F. Kiang, "Effect of mutual coupling on the channel capacity of MIMO systems," *IEEE Trans. Veh. Technol.*, vol. 65, no. 1, pp. 398–403, Jan. 2016.
[46] S. Luo, Y. Zhang, G. F. Pedersen, and S. Zhang, "Mutual decoupling for massive MIMO antenna arrays by using triple-layer meta-surface," *IEEE Open J. Antennas Propag.*, vol. 3, pp. 1079–1089, 2022.
[47] K.-L. Wu, C. Wei, X. Mei, and Z.-Y. Zhang, "Array-antenna decoupling surface," *IEEE Trans. Antennas Propag.*, vol. 65, no. 12, pp. 6728–6738, Dec. 2017.
[48] M. Li, X. Chen, A. Zhang, A. A. Kishk, and W. Fan, "Reducing correlation in compact arrays by adjusting near-field phase distribution for MIMO applications," *IEEE Trans. Veh. Technol.*, vol. 70, no. 8, pp. 7885–7896, Aug. 2021.
[49] C. Wei, Z. Zhang, and K. Wu, "Phase compensation for decoupling of large-scale staggered dual-polarized dipole array antennas," *IEEE Trans. Antennas Propag.*, vol. 68, no. 4, pp. 2822–2831, Apr. 2020.

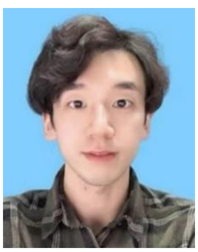

ZHANG WEN CHENG received the B.S. degree from Zhengzhou University, Zhengzhou, China, in 2019. He is currently pursuing the Ph.D. degree in electromagnetic field and microwave technology with Southeast University, Nanjing, China.

His current research interests include leaky-wave antennas, spoof surface plasmon polaritons, and metamaterials.

SHIMENG WANG received the B.S. degree from Beijing Jiaotong University, Beijing, China, in 2015, and the Ph.D. degree from The University of Manchester, Manchester, U.K., in 2020.

Since 2021, he has been working with the China Mobile R&D Center for Network Planning and Optimization, China Mobile Group Design Institute Company Ltd., Beijing, China. His current research interests include network optimization with spoof surface plasmon polaritons and metamaterials.

YUE TENG CHEN received the B.E. and M.S. degrees from the University of Electronic Science and Technology of China, Chengdu, China, in 2018 and 2021, respectively. He is currently pursuing the Ph.D. degree in electromagnetic field and microwave technology with the State Key Laboratory of Millimeter Waves, Southeast University, Nanjing, China.

His research fields spot on programmable metasurface, antenna array, and beam forming.

JI RAN CHEN received the B.S. degree from Southwest Jiaotong University, Chengdu, China, in 2021. He is currently pursuing the M.S. degree in electromagnetic field and microwave technology with Southeast University, Nanjing, China.

His current research interests include spoof surface plasmon polaritons and leaky-wave antennas.

JING CHENG LIANG received the B.E. degree from the School of Electronic Science and Engineering, Nanjing University of Posts and Telecommunications, Nanjing, China, in 2016, and the M.E. degree from the School of Electronic Science and Engineering, University of Electronic Science and Technology of China, Chengdu, China, in 2019. He is currently pursuing the Ph.D. degree with the State Key Laboratory of Millimeter Waves, Southeast University, Nanjing.

His current research interests include metasurfaces and reconfigurable intelligent surface.

FENG GAO received the B.S. and M.S. degrees from Air Force Engineering University, Xi'an, China, in 1996 and 1999, respectively, and the Ph.D. degree from Xidian University, Xi'an, in 2008.

Since 2018, he has been working with the China Mobile R&D Center for Network Planning and Optimization, China Mobile Group Design Institute Company Ltd., Beijing, China. His current research interests include network optimization and antenna techniques.

SHUAI LUAN received the B.S. and M.S. degrees from Southwest Jiaotong University, Chengdu, China, in 2004 and 2007, respectively.

Since 2020, he has been working with the China Mobile R&D Center for Network Planning and Optimization, China Mobile Group Design Institute Company Ltd., Beijing, China. His current research interests include mobile network optimization intelligent hardware and antenna techniques.

XIN LIU received the B.S. degree from the Beijing Institute of Technology, Beijing, China, in 2000.

Since 2018, he has been working with the China Mobile R&D Center for Network Planning and Optimization, China Mobile Group Design Institute Company Ltd, Beijing. His current research interests include network optimization with spoof surface plasmon polaritons and metamaterials.

HUI FENG MA (Member, IEEE) received the B.S. degree in electronic engineering from the Nanjing University of Science and Technology, Nanjing, China, in 2004, and the Ph.D. degree from the State Key Laboratory of Millimeter Waves, Southeast University, Nanjing, in 2010.

In 2010, he joined the School of Information Science and Engineering, Southeast University, and was promoted to an Associate Professor in 2011 and a Full Professor in 2015. He was selected as a Jiangsu Specially Appointed Professor in 2021. His current research interests include metasurface, spoof surface plasmon polaritons, and metamaterial circuits and antennas. He was a recipient of the Second Prize of National Award for Natural Science, China, in both 2014 and 2018, and the First Prize of Natural Science from the Ministry of Education, China, in 2011. His research of 3-D ground carpet cloak realized by using metamaterials was selected as one of the "10 Breakthroughs of Chinese Science in 2010."

TIE JUN CUI (Fellow, IEEE) received the B.Sc., M.Sc., and Ph.D. degrees in electrical engineering from Xidian University, Xi'an, China, in 1987, 1990, and 1993, respectively.

In March 1993, he joined the Department of Electromagnetic Engineering, Xidian University, where he was promoted to an Associate Professor in November 1993. From 1995 to 1997, he was a Research Fellow with the Institut fur Hochstfrequenztechnik und Elektronik, University of Karlsruhe, Karlsruhe, Germany. In July 1997, he joined the Center for Computational Electromagnetics, Department of Electrical and Computer Engineering, University of Illinois at Urbana–Champaign, Champaign, IL, USA, first as a Postdoctoral Research Associate and then as a Research Scientist. In September 2001, he was a Cheung-Kong Professor with the Department of Radio Engineering, Southeast University, Nanjing, China, where he is currently a Chief Professor and the Founding Director of the Institute of Electromagnetic Space. He is the first author of books *Metamaterials–Theory, Design, and Applications* (Springer, November 2009); *Metamaterials: Beyond Crystals, Noncrystals, and Quasicrystals* (CRC Press, March 2016), and *Information Metamaterials* (Cambridge University Press, 2021). He has published over 500 peer-reviewed journal articles, which have been cited by more than 39000 times (H-Factor 98; Google Scholar), and licensed over 100 patents. His research interests include metamaterials and computational electromagnetics. He proposed the concepts of digital coding and programmable metamaterials, and realized their first prototypes, based on which he founded the new direction of information metamaterials, bridging the physical world and digital world.

Dr. Cui was a recipient of the Research Fellowship from the Alexander von Humboldt Foundation, Bonn, Germany, in 1995; the Young Scientist Award from the International Union of Radio Science in 1999; the Cheung Kong Professor by the Ministry of Education, China, in 2001; the National Science Foundation of China for Distinguished Young Scholars in 2002; the Natural Science Award (first class) from the Ministry of Education, China, in 2011, and the National Natural Science Awards of China (second class, twice), in 2014 and 2018. His research has been selected as one of the most exciting peer-reviewed optics research "Optics in 2016" by *Optics and Photonics News Magazine*, Ten Breakthroughs of China Science in 2010, and many research highlights in a series of journals. His work has been widely reported by *Nature News, MIT Technology Review, Scientific American, Discover,* and *New Scientists*. From 2019 to 2021, he was ranked in the top 1% for the highly cited papers in the field of Physics by Clarivate Web of Science (Highly Cited Researcher). He served as an Associate Editor for IEEE TRANSACTION ON GEOSCIENCE AND REMOTE SENSING and a Guest Editor for *Science China Information Sciences, Science Bulletin*, IEEE JOURNAL ON EMERGING AND SELECTED TOPICS IN CIRCUITS AND SYSTEMS, and *Research*. He is also a Chief Editor of Short Book *Metamaterial* (Cambridge University Press), an Editor of *Materials Today Electronics*, an Associate Editor of *Research*, and an Editorial Board Member of *National Science Review*, *eLight*, *PhotoniX*, *Advanced Optical Materials*, *Small Structure*, and *Advanced Photonics Research*. He presented more than 60 Keynote and Plenary Talks in academic conferences, symposiums, or workshops. He is also an Academician of the Chinese Academy of Science.